Note that the axes are changed such that e'/d' is calculated according to $e'/d' = e/d\sqrt{27/20} \sim 1.71$ (with $e/d = 145/98$ derived from the section).

Fig. 7 shows an example of an histological section and a corresponding hexagon (a) from which the error functions are calculated (see below). In the next step the section is sheared by $\Delta/a = 0.1$ where the outer contour of the original section is superimposed (b). As can be seen, alignment is worsened when the PAT has been applied (c). This condition can be attributed mainly to a rotational error of $\sim 3.5^\circ$ corresponding to ~ 8 pixels at the outer contour. This finding is in good agreement with the expected $\sim 3.3^\circ$ calculated from the theoretical analysis.

III. Conclusion

For precise alignment, the PAT can account for at most $1/2n(n+1)$ parameters in n dimensions, since the inertia matrices are symmetrical. The number of equations is, therefore, not sufficient for an exact alignment of objects that can be related by an affine transformation with n^2 parameters (without translation).

An analytical model is devised for determining the error functions when the PAT is used in the presence of shearing parameters. With this analytical model, misalignment can be decomposed into rotational and scaling errors which can be examined by varying the shearing and form parameters. The theory shows, that minute shearing results in strong rotational error if the shapes are approximately square, but scaling errors dominate in cases with extensive shearing. With increasingly rectangular shapes, the rotational error decreases for a fixed shearing parameter. The study also reveals misalignment if the PAT reported in [1] is applied, demonstrating that stabilizing modifications of (6) are required.

References

[1] R. Bajcsy and S. Kovacic, "Multiresolution elastic matching," *Comput. Vision Graph Image Processing*, vol. 46, pp. 1–21, 1989.

[2] L. S. Hibbard and R. A. Hawkins, "Objective image alignment for 3-D reconstruction of digital autoradiograms," *J. Neurosci. Meth.*, vol. 26, pp. 55–74, 1988.

[3] A. W. Toga and P. K. Banerjee, "Registration revisited," *J. Neurosci. Meth.*, vol. 48, pp. 1–13, 1993.

[4] I. Kapouleas, A. Alavi, W. M. Alves, R. E. Gur, and D. W. Weiss, "Registration of three-dimensional MR and PET images of the human brain without markers," *Radiol.*, vol. 181, pp. 731–739, 1991.

[5] N. M. Alpert, J. F. Bradshaw, D. Kennedy, and J. A. Correia, "The principal axes transformation—A method for image registration," *J. Nucl. Med.*, vol. 31, pp. 1717–1722, 1990.

[6] E. J. Holupka and H. M. Kooy, "A geometric algorithm for medical image correlations," *Med. Phys.*, vol. 19, pp. 433–438, 1992.

[7] M. K. Hu, "Visual pattern recognition by moment invariants," *IEEE Trans. Inform. Theory*, pp. 179–189, Feb. 1962.

[8] G. Fischer, *Analytische Geometrie.* Braunschweig, Germany: Vieweg & Sohn, 1979.

[9] T. Schormann, A. Dabringhaus, and K. Zilles, "Extension of the principal axes theory for the determination of affine transformations," in *Proceedings of the DAGM: Informatik-Aktuell.* Berlin, Germany: Springer-Verlag, 1997, pp. 384–391.

Automatic Detection of the Mid-Sagittal Plane in 3-D Brain Images

Babak A. Ardekani,* Jeff Kershaw, Michael Braun, and Iwao Kanno

***Abstract*—This article presents a detailed description of an algorithm for the automatic detection of the mid-sagittal plane in three-dimensional (3–D) brain images. The algorithm seeks the plane with respect to which the image exhibits maximum symmetry. For a given plane, symmetry is measured by the cross-correlation between the image sections lying on either side. The search for the plane of maximum symmetry is performed by using a multiresolution approach which substantially decreases computational time. The choice of the starting plane was found to be an important issue in optimization. A method for selecting the initial plane is presented. The algorithm has been tested on brain images from various imaging modalities in both humans and animals. Results were evaluated by visual inspection by neuroradiologists and were judged to be consistently correct.**

***Index Terms*—Brain, image registration, medical imaging, mid-sagittal plane, pattern recognition.**

I. Introduction

This paper describes a robust algorithm for the automatic detection of the mid-sagittal plane (MSP) in arbitrarily oriented three-dimensional (3-D) brain images.

The algorithm has several useful applications. MSP detection is often the first step in spatial normalization or anatomical standardization of brain images [1], [2]. It is also a useful first step in intrasubject inter/intramodality image registration [3], where aligning the MSP's between images reduces the degrees of freedom to three (one rotation and two translations). This simplifies the problem to one of two-dimensional (2-D) registration which can be achieved by whatever technique is most appropriate. The algorithm is also useful for defining symmetric regions of interest in left and right hemispheres. In single photon emission tomography (SPECT) for example, this allows accurate comparison of the local radionuclide uptake in opposing sides of the brain where any observed asymmetry may be useful for clinical diagnosis [4].

Several papers in the medical imaging literature have previously considered this problem [5]–[7]. Junck *et al.* [5] developed a method for automatic detection of the *line* of symmetry in a transverse positron emission tomography (PET) or SPECT slice. The two parameters that specify the line of symmetry are found by an exhaustive search. An exhaustive search is really only computationally feasible for 2-D cases and when the initial guess for the orientation of the line of symmetry is close to the optimum. We have found in practice that the cross-correlation method as presented in [5] does not reliably locate the MSP in three dimensions.

Manuscript received July 30, 1997; revised November 4, 1997. The work of B. A. Ardekani was supported by the Japan Science and Technology Agency under an STA Postdoctoral Research Fellowship. The Associate Editor responsible for coordinating the review of this paper and recommending its publication was M. W. Vannier. *Asterisk indicates corresponding author.*

*B. A. Ardekani is with the Department of Radiology and Nuclear Medicine, Research Institute for Brain and Blood Vessels, 6-10 Senshu-kubota machi, Akita 010, Japan (e-mail: babak@akita-noken.go.jp).

J. Kershaw and I. Kanno are with the Department of Radiology and Nuclear Medicine, Research Institute for Brain and Blood Vessels, Akita 010, Japan.

M. Braun is with the Department of Applied Physics, University of Technology, Sydney 2007 Australia.

Publisher Item Identifier S 0278-0062(97)09343-9.

Minoshima *et al.* [6] presented a method for detecting the MSP in 3-D PET images. The measure of symmetry used in this paper is a modified stochastic sign change (SSC) criterion [8]. This paper also relies on an exhaustive search of a small region of the parameter space for the optimal MSP. By limiting the search to this region, they are assuming that the scans are very close to being either coronal or transaxial.

Neither [5] nor [6] applied their algorithms to MR images. On the other hand, Brummer's approach [7] is suitable for MR images only. The technique is based on a Hough transform of edge images obtained using Sobel edge detectors and therefore is only suited for high-resolution images such as MR images. It also requires transaxial or coronal scans and will not work with sagittal scans, essentially reducing the problem to finding mid-sagittal lines in 2-D slices.

The approach presented in this paper is based on the premise that the MSP separates a 3-D brain image into two almost symmetric halves. We define a criterion to measure symmetry and find the plane that maximizes this criterion. This is basically the same approach used in [5] and [6], but we have overcome some of the restrictions of these works. More precisely, we need make no particular assumption about the scan orientation, nor are we restricted to a specific imaging modality. The algorithm is truly 3-D and is insensitive to how the data is initially presented to the program—we can arbitrarily rotate and translate the image set in three dimensions and still obtain the desired result. This is possible because we have introduced some new ideas for overcoming the problem of local minima in the similarity measure. Specifically, a multiresolution approach is adopted whereby an approximate location of the MSP is constructed from smaller images of lower resolution and then located more accurately in images with higher resolution. This improves the computational efficiency of the algorithm and is the reason why we can perform the true 3-D algorithm within a reasonable time period.

The paper is organized as follows. In Section II, we present a concise mathematical formulation of the theory and describe the implementation of the algorithm in detail. In Section III, we apply the method to a large number of images and evaluate the results. Discussion is presented in Section IV followed by conclusions in Section V.

II. Methods

A. Measure of Symmetry

Consider three sets of integers $I = \{0, 1, \cdots, N_x - 1\}$, $J = \{0, 1, \cdots, N_y - 1\}$, and $K = \{0, 1, \cdots, N_z - 1\}$. Let $\mathcal{D}$ denote the product set of I, J, and K, that is

$$\mathcal{D} = I \times J \times K = \{(i, j, k): i \in I, j \in J, k \in K\}. \tag{1}$$

A 3-D medical image can be considered as a function f that maps $\mathcal{D}$ into the set of real numbers $\mathbb{R}$. Points (i, j, k) represent *volume elements* (voxels). The image value or intensity at a voxel (i, j, k) is denoted by $f(i, j, k)$. Alternatively, the image may be represented by an N-dimensional vector $\mathbf{f}$ ($N = N_x \times N_y \times N_z$) with elements $f_n = f(i, j, k)$, where $n = k\,N_x\,N_y + j\,N_x + i$ ($n = 0, 1, \cdots, N - 1$).

The array of numbers $f(i, j, k)$ represents discrete samples of a function $f_c(x, y, z)$ defined on a continuous domain $\mathcal{C} \subset \mathbb{R}^3$. More precisely, we define $f(i, j, k) = f_c(x_i, y_j, z_k)$ with

$$\begin{aligned} x_i &= [i - (N_x - 1)/2]\, d_x \\ y_j &= [j - (N_y - 1)/2]\, d_y \\ z_k &= [k - (N_z - 1)/2]\, d_z. \end{aligned} \tag{2}$$

The quantities d_x, d_y, and d_z are the sampling intervals (voxel dimensions) in the x, y, and z directions, respectively. Note that distances in $\mathcal{C}$ are real-world distances in units of millimeters (mm).

Points $(x, y, z) \in \mathcal{C}$ are related to precise locations within the *field of view* (FOV) of the scanner by adopting the following conventions. The origin is taken to be at the center of the FOV. The z direction is assumed to lie parallel to the axis of the scanner. The x and y axes are chosen as left to right, and anterior to posterior directions, respectively.

The equation of a plane in three dimensions can be written in the form

$$F(x, y, z) = ax + by + cz - 1 = 0. \tag{3}$$

Each plane is characterized by a unique set of parameters (a, b, c). Our aim is to find the triplet (a, b, c) with respect to which the image $\mathbf{f}$ has maximum "symmetry."

To determine the symmetry of $\mathbf{f}$, [5] and [6] compare it with the image $\mathbf{g}$ that is obtained when $\mathbf{f}$ is reflected (flipped) about the plane. The measure of symmetry used in [6] is the SSC criterion computed for $\mathbf{f} - \mathbf{g}$. The measure of symmetry used in [5] is the cross-correlation between $\mathbf{f}$ and $\mathbf{g}$ defined as

$$s(\mathbf{f}, \mathbf{g}) = \frac{(\mathbf{f} - \overline{f}\mathbf{1}).(\mathbf{g} - \overline{g}\mathbf{1})}{\|(\mathbf{f} - \overline{f}\mathbf{1})\|\,\|(\mathbf{g} - \overline{g}\mathbf{1})\|} \tag{4}$$

where $\overline{f}$ and $\overline{g}$ are the means of the elements of $\mathbf{f}$ and $\mathbf{g}$, respectively, and $\mathbf{1}$ is an N-dimensional vector with all its elements equal to one.

The present paper also uses the cross-correlation symmetry measure. However, the cross correlation is computed between two modified vectors $\mathbf{f}'$ and $\mathbf{g}'$. There are two modifications. First, $\mathbf{f}'$ only consists of voxels on the positive side of the plane [$F(x, y, z) > 0$], while $\mathbf{g}'$ only consists of voxels on the negative side of the plane [$F(x, y, z) < 0$]. This is in contrast with the definitions of $\mathbf{f}$ and $\mathbf{g}$ used in (4) where $\mathbf{f}$ is the entire image and $\mathbf{g}$ is its reflection about a presumed MSP. The second modification ensures that all elements of $\mathbf{f}'$ and $\mathbf{g}'$ are greater than a given threshold level T. This is achieved by removing all elements n from both $\mathbf{f}$ and $\mathbf{g}$ if either $\mathbf{f}_n$ or $\mathbf{g}_n$ is less than or equal to T. The procedure for obtaining $\mathbf{f}'$ and $\mathbf{g}'$ is as follows.

1) For each point $(i, j, k) \in \mathcal{D}$, compute the corresponding point $\mathbf{P} = (x_i, y_j, z_k) \in \mathcal{C}$ from (2). Proceed if $f(i, j, k) > T$ and $F(\mathbf{P}) > 0$. Otherwise, skip (i, j, k) and process the next point.
2) Find the reflection of point $\mathbf{P}$ with respect to the plane by
$$\mathbf{P}' = (x_i', y_j', z_k') = \mathbf{P} - 2\frac{F(\mathbf{P})}{\|\nabla F\|}\frac{\nabla F}{\|\nabla F\|}. \tag{5}$$
3) If $\mathbf{P}'$ falls outside the FOV, set $g(i, j, k) = 0$. Otherwise, set $g(i, j, k) = \hat{f}_c(x_i', y_j', z_k')$ where $\hat{f}_c(x_i', y_j', z_k')$ is an estimate of f_c at $\mathbf{P}'$ obtained by interpolation.
4) If $g(i, j, k) > T$, include $f(i, j, k)$ in $\mathbf{f}'$ and $g(i, j, k)$ in $\mathbf{g}'$.

Note that *both* the original and reflected points, $f_c(\mathbf{P})$ and $\hat{f}_c(\mathbf{P}')$, must exceed the threshold T in order to be included in $\mathbf{f}'$ and $\mathbf{g}'$.

Using the modified vectors $\mathbf{f}'$ and $\mathbf{g}'$ has the obvious advantage of improving computational efficiency since the size of the vectors is substantially smaller than N. More importantly, $s(\mathbf{f}', \mathbf{g}')$ is a more useful measure of symmetry than (4) for detection of the MSP. We shall present our arguments for this in Section IV.

B. Reduction of the Image Size

The search for the MSP in three dimensions is computationally expensive. The computation time is proportional to the number of image voxels and can be substantially shortened by a multiresolution

approach which uses images of smaller dimension. This section outlines our algorithm for performing the image reduction.

Let the original image matrix size be $N_x \times N_y \times N_z$ voxels, and the dimensions of each voxel $d_x \times d_y \times d_z$ mm^3. The resizing is performed so that the resulting voxels are almost cubic. We first specify the dimension N'_x ($<N_x$) of the new matrix. The corresponding voxel dimension d'_x for the new image is calculated as

$$d'_x = d_x \times (N_x - 1)/(N'_x - 1). \tag{6}$$

This is used to obtain the y and z dimensions of the new matrix

$$\begin{aligned} N'_y &= \mathrm{RU}\left[d_y \times (N_y - 1)/d'_x + 1\right] \\ N'_z &= \mathrm{RU}\left[d_z \times (N_z - 1)/d'_x + 1\right] \end{aligned} \tag{7}$$

where we use the notation "RU" to indicate rounding up to the nearest integer. From N'_y and N'_z the new voxel dimensions d'_y and d'_z are obtained in the same manner as (6). They are equal to or slightly less than d'_x so that the voxels in the new image are *almost* cubic.

With the dimensions for the matrix and voxels of the reduced image finalized, we can proceed to resampling. This is a two-step process. The first step is to use a Gaussian kernel to smooth the original image. Since a Gaussian kernel is separable, smoothing with a 3-D kernel is equivalent to smoothing with three one-dimensional (1-D) kernels. The 1-D kernel for the x direction is given by

$$h_c(x) = \frac{1}{\sqrt{2\pi\sigma_x^2}} \exp\left(\frac{-x^2}{2\sigma_x^2}\right). \tag{8}$$

The parameter σ_x determines the amount of smoothing in the x direction. A larger σ_x results in a greater degree of smoothing. The image scanner is assumed to have a Gaussian point spread function (PSF) in the x direction, with full-width half-maximum (FWHM) equal to $r \times d_x$. We choose σ_x so that the ratio r is maintained between the FWHM of the reduced image and its voxel dimension d'_x. This means we must satisfy

$$\sigma_x^2 = \frac{r^2}{8 \ln 2}\left(d'^2_x - d_x^2\right). \tag{9}$$

In our implementation we assume a value of two for r. The smoothing kernels for the y and z directions are constructed in the same way. Once the smoothing kernels are known, they are used to smooth the original image by a series of 1-D discrete convolutions.

If the PSF of the scanner is not Gaussian, but can be at least approximated by some other analytic form, then a similar but possibly more complicated equation may be derived for σ_x^2. In such cases, it may be simpler to regard (9) as an *ad hoc* rule for choosing the smoothing kernel used to reduce image resolution. The only consequence of such an approximation is that the ratio between the FWHM of the smoothed image and d'_x is not necessarily equal to r. This will not interfere with the effectiveness of the algorithm since r is not a critical factor in the method.

The second step in the resampling process is to select voxel values for the smaller $N'_x \times N'_y \times N'_z$ image from the smoothed image. We apply linear interpolation for this task.

The following are some practical points concerning the implementation of the algorithm.

1) Since the domain of the kernel in (8) is $(-\infty, \infty)$, we truncate it by setting $h(x) = 0$ for $|x| > 1.65\sigma_x$ mm. This makes the area under the truncated portion of the curve less than 1%. The discrete version of $h_c(x)$ which is used in computations is

$$h(i) = \alpha h_c(id_x) \qquad i = 0, \pm 1, \pm 2, \cdots \tag{10}$$

where α is a normalizing constant chosen to make $\sum_i h(i) = 1$.

2) Care must be taken when computing the 1-D convolutions near the image boundaries since the convolution kernel and the image matrix do not completely overlap in these regions. The difficulty is overcome by extending the image beyond its boundaries by mirror reflections.
3) If the choice of N'_x results in either $N'_y > N_y$ or $N'_z > N_z$, then we do not perform the Gaussian smoothing in that direction.

C. Optimization

This section outlines the method used for maximizing the similarity measure $s(\mathbf{f}', \mathbf{g}')$ defined in (4) with respect to the parameters $\mathbf{u} = (a, b, c)$. Note that s is only implicitly dependent on (a, b, c) through $\mathbf{f}'$ and $\mathbf{g}'$. The basic procedure is simple. We start at an initial point $\mathbf{u}_0$ in the parameter space and find a local maximum of $s(\mathbf{f}', \mathbf{g}')$ using an optimization algorithm. Whether or not this local maximum corresponds to the MSP is dependent on the choice of starting point. Thus, choosing $\mathbf{u}_0$ is an important issue.

The "center of mass" of an image is defined as follows:

$$\begin{aligned} x_{\mathrm{cm}} &= \frac{1}{M} \sum_{(i,j,k)\in\mathcal{D}} x_i f(i, j, k) \\ y_{\mathrm{cm}} &= \frac{1}{M} \sum_{(i,j,k)\in\mathcal{D}} y_j f(i, j, k) \\ z_{\mathrm{cm}} &= \frac{1}{M} \sum_{(i,j,k)\in\mathcal{D}} z_k f(i, j, k) \end{aligned}$$

where

$$M = \sum_{(i,j,k)\in\mathcal{D}} f(i, j, k) \tag{11}$$

x_i, y_j, and z_k are as in (2), and $f(i, j, k)$ is the image value at voxel (i, j, k). In most cases the MSP will pass near this point, hence it is reasonable to choose $\mathbf{u}_0$ from amongst the set of planes which contain the center of mass. Now consider a sphere of unit radius centered at $\mathbf{P}_{\mathrm{cm}} = (x_{\mathrm{cm}}, y_{\mathrm{cm}}, z_{\mathrm{cm}})$. Any point $\mathbf{P}$ on the sphere uniquely defines a plane. Specifically, the plane passes through point $\mathbf{P}_{\mathrm{cm}}$ with unit normal $\mathbf{P} - \mathbf{P}_{\mathrm{cm}}$. Our procedure is to select Q points on the unit sphere and evaluate $s(\mathbf{f}', \mathbf{g}')$ for all of the corresponding planes. The initial plane $\mathbf{u}_0$ is then chosen as the one which returns the largest value. The following procedure is used for specifying the Q points.

1) Set $i = 1$ and let $\Delta\phi = \pi/(2q)$ where q is a given integer.
2) In spherical coordinates a point on the unit sphere can always be specified by the two angles ϕ and θ, $0 \leqslant \phi \leqslant \pi$, $0 \leqslant \theta \leqslant 2\pi$. Define $\phi_i = i\Delta\phi$. Select RU$[q \sin \phi_i]$ points at equal distances on the semicircle at $\phi = \phi_i$ and $\alpha \leqslant \theta \leqslant \alpha + \pi$, where α is an angle between 0 and 2π chosen at random.
3) If $i < q$, increase i by one and repeat Step 1. Note that when $i = q$, $\phi_i = \pi/2$ and RU$[q \sin \phi_i] = q$. Therefore, q is the number of points that would be selected on the largest semicircle defined by $\phi = \pi/2$ and $\alpha \leqslant \theta \leqslant \alpha + \pi$.
4) Select the additional point $\phi = 0$ on the unit sphere.

Recall that the notation "RU" indicates rounding up to the nearest integer. The number of points selected is a function of the given parameter q. For example, $q = 20$ gives $Q = 138$. Evaluating $s(\mathbf{f}', \mathbf{g}')$ for all Q points would normally be computationally expensive. This problem is overcome by using images of reduced resolution and dimension obtained by implementing the image reduction scheme outlined in the previous subsection.

After choosing the starting point $\mathbf{u}_0$, we obtain a local maximum of $s(\mathbf{f}', \mathbf{g}')$ by applying the downhill simplex optimization method

[9]. Our choice of the optimization method was not based on any particular reasoning. We have found that this method works quite well and gives satisfactory results. In order to speed up the optimization process, we first maximize $s(\mathbf{f}', \mathbf{g}')$ at a reduced image scale. The process is then repeated at a larger image scale starting at the optimum point found by the previous step. This process can be applied any number of times, but in practice, we have obtained accurate results with only a two step process.

One other important issue regarding the maximization process is the existence of degenerate solutions (a, b, c) where it is possible for $s(\mathbf{f}', \mathbf{g}')$ to take on large values. For example, if the plane (a, b, c) passes near the head boundary, $\mathbf{f}'$ and $\mathbf{g}'$ will contain relatively few points which are spatially close. If the image intensity does not vary appreciably within $\mathbf{f}'$ and $\mathbf{g}'$, then $s(\mathbf{f}', \mathbf{g}')$ will produce a large value which is not of interest. If this problem is not dealt with, the optimization routines frequently find such degenerate solutions. A simple way to overcome this problem is to constrain the search space to those planes for which the number of elements in $\mathbf{f}'$ is greater than a certain percentage of the number of elements in the set $\{(i, j, k) \in \mathcal{D}\colon f(i, j, k) > T\}$, where $\mathcal{D}$ is as defined in (1) and T is the given threshold level.

III. Results

In order to evaluate the performance of the automatic MSP detection algorithm, it was applied to brain images from 20 patients arbitrarily selected from amongst a pool of images available in the picture archiving and communication system (PACS) at the Research Institute for Brain and Blood Vessels (Akita, Japan). All patients had both O^{15}-water PET and T1-weighted magnetic resonance imaging (MRI) scans. Nine patients also had T2-weighted MRI scans. The PET images were of matrix dimension $128 \times 128 \times 46$ and voxel dimension $2.0 \times 2.0 \times 3.125$ mm^3, whereas the MRI scans were of matrix dimension $256 \times 256 \times 19$ with voxel dimension $1.01 \times 1.01 \times 6.0$ mm^3.

As mentioned in Section II, the algorithm uses images of reduced resolution and size in order to speed up the computations. The scale of the image that was used in the procedure for finding the starting plane $\mathbf{u}_0$ was specified by selecting $N'_x = 32$. This resulted in a matrix size of $32 \times 32 \times 18$ in the case of PET images and $32 \times 32 \times 14$ for the MR images. The value of the parameter q was chosen to be 50 resulting in a Q of 818. The same size images were used in the first stage of the optimization process. In the second stage, N'_x was set to 64, making the PET and MR image dimensions $64 \times 64 \times 36$ and $64 \times 64 \times 27$, respectively. The value of the threshold parameter T used in defining $\mathbf{f}'$ and $\mathbf{g}'$ was selected to be zero. This eliminates the negative values in the PET image which are artifacts of the reconstruction algorithm. For both our MRI and PET images $T = 0$ eliminates most of the background points, although the threshold can be arbitrarily increased if necessary, particularly if there are large background values in nonbrain regions in the PET data. In order to prevent the optimization algorithm from finding the type of degenerate solutions mentioned in Section II-C, the search space was constrained to those planes for which the number of elements in $\mathbf{f}'$ is at least 20% of the number of elements in the set $\{(i, j, k) \in \mathcal{D}\colon f(i, j, k) > T\}$.

The algorithm was implemented in C on a Silicon Graphics INDY R5000 workstation. For the parameter values given above, the average computing times were approximately 45 and 35 s in PET and MR images, respectively.

The results from all 49 image volumes were inspected by expert neuroradiologists and in 47 cases were judged to be highly accurate. Fig. 1 contains example slices from the successful cases. The two image volumes for which the algorithm failed were in fact the PET and MRI scan from the same patient. Fig. 2 shows MRI slices from this subject with the detected plane of maximum symmetry overlaid. This patient was a 58-year-old man who suffered from a transit ischemic attack and had an operation of the anastomosis between the superficial temporal artery and the middle cerebral artery. The MRI scan was performed two days after the operation. Quite clearly, the failure of the algorithm in this case is caused by the high degree of asymmetry which is present in the image.

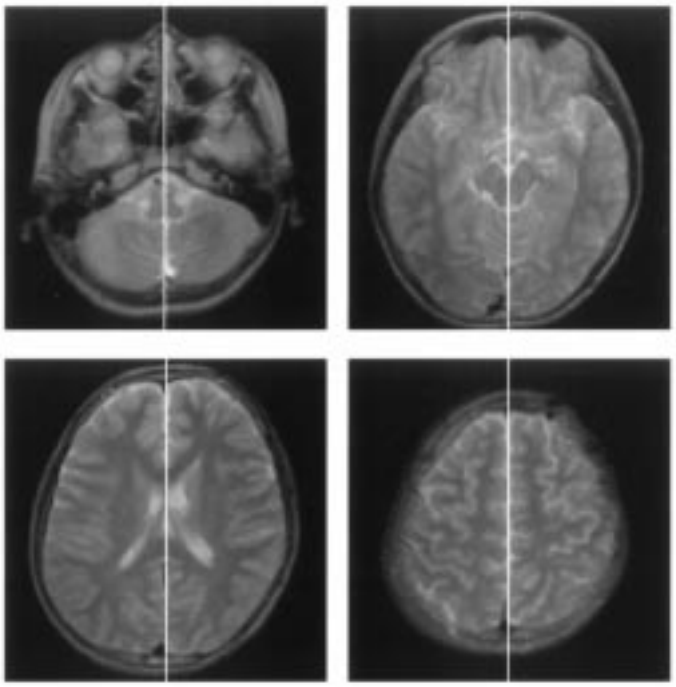

(a)

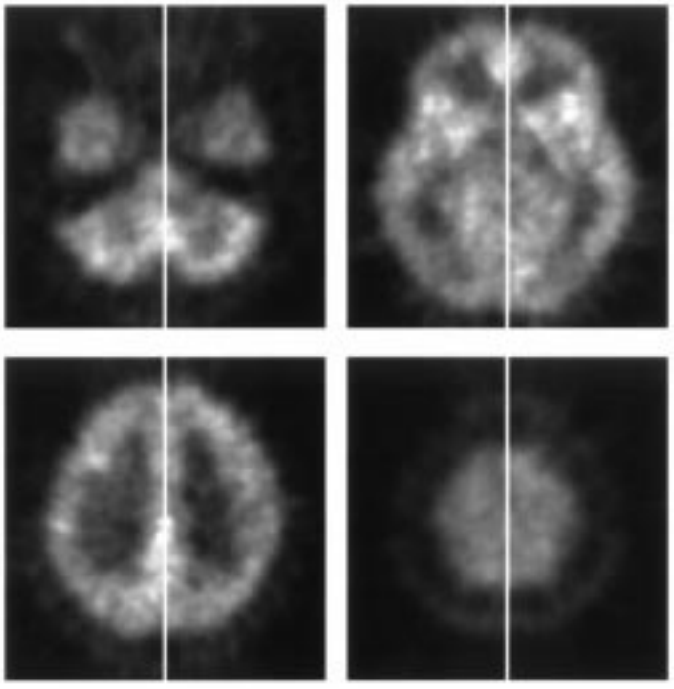

(b)

Fig. 1. Examples of successful searches for the MSP in (a) T2-weighted MRI and (b) O^{15}-water PET images.

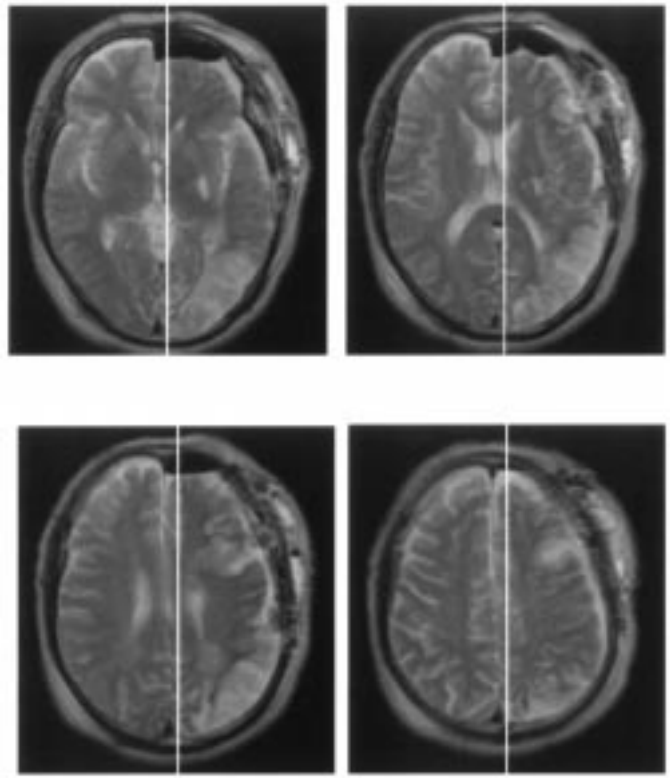

Fig. 2. Slices from the MR image where the algorithm failed. This patient was a 58-year-old man who suffered from a transit ischemic attack and had an operation of the anastomosis between the superficial temporal artery and the middle cerebral artery. The MRI scan was performed two days after the operation.

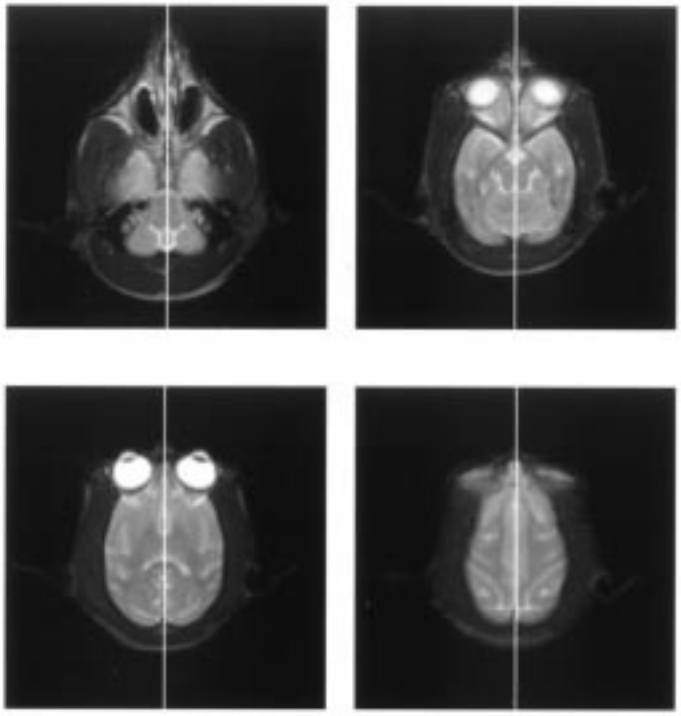

Fig. 3. Slices from an MRI study of a monkey showing the successfully located MSP.

We have also successfully tested the algorithm on PET and MRI scans from cats and monkeys. Fig. 3 shows the MSP detected in an MR image volume from a monkey. In animal experiments, the results were used in MR-PET registration to reduce the number of parameters required for full alignment from six to three.

IV. Discussion

In Section II-A, it was stated that the measure of symmetry $s(\mathbf{f}', \mathbf{g}')$ used in this paper is more useful than $s(\mathbf{f}, \mathbf{g})$. To justify this statement, first note that if we ignore interpolation errors in the construction of $\mathbf{g}$, then $\overline{g} = \overline{f}$ = constant and $\|\mathbf{f}\| = \|\mathbf{g}\|$ = constant. From these relations, it can be easily deduced that maximizing $s(\mathbf{f}, \mathbf{g})$ is equivalent to simply maximizing $\mathbf{f}.\mathbf{g}$. Furthermore, through the identity

$$\|\mathbf{f} - \mathbf{g}\|^2 = 2(\|\mathbf{f}\|^2 - \mathbf{f}.\mathbf{g}) \tag{12}$$

it is equivalent to minimizing $\|\mathbf{f}-\mathbf{g}\|^2$, the sum of squared differences between elements of $\mathbf{f}$ and $\mathbf{g}$. Let us consider the problem in terms of this latter function.

The sum of squared differences $\|\mathbf{f} - \mathbf{g}\|^2$ is computed over set $\mathcal{D}$. Set $\mathcal{D}$ can be divided into three regions

$$\begin{aligned}
\mathcal{D}_1 &= \{(i, j, k) \in \mathcal{D}\colon f(i, j, k) > T,\ g(i, j, k) > T\} \\
\mathcal{D}_2 &= \{(i, j, k) \in \mathcal{D}\colon f(i, j, k) \leqslant T,\ g(i, j, k) \leqslant T\} \\
\mathcal{D}_3 &= \mathcal{D} - \mathcal{D}_1 \cup \mathcal{D}_2.
\end{aligned} \tag{13}$$

Thus, using the linearity of $\|\ \|^2$, $\|\mathbf{f} - \mathbf{g}\|^2$ can be broken into three terms

$$\|\mathbf{f} - \mathbf{g}\|^2 = \|\mathbf{f} - \mathbf{g}\|^2_{\mathcal{D}_1} + \|\mathbf{f} - \mathbf{g}\|^2_{\mathcal{D}_2} + \|\mathbf{f} - \mathbf{g}\|^2_{\mathcal{D}_3}. \tag{14}$$

Fig. 4(a) and (b) schematically illustrate the problem that can occur when $s(\mathbf{f}, \mathbf{g})$ is used. The image $\mathbf{f}$ (thick boundary) is deliberately chosen to be asymmetric by removing a part of the "brain." The reflected image $\mathbf{g}$ is also shown (thin boundary). The intensity of the image in the brain region is assumed to be relatively constant. The values of $\mathbf{f} - \mathbf{g}$ along the cross-section AB are also sketched.

The images $\mathbf{f}$ and $\mathbf{g}$ over $\mathcal{D}_2$ only consist of background voxels. Therefore, the sum of squares in this region, $\|\mathbf{f} - \mathbf{g}\|^2_{\mathcal{D}_2}$, is assumed to be small. Clearly a large contribution to $\|\mathbf{f} - \mathbf{g}\|^2$ will come from region $\mathcal{D}_3$. In this situation, in order to minimize $\|\mathbf{f} - \mathbf{g}\|^2$, the optimization algorithm may drive the MSP away from the true position in order to reduce the contribution from $\|\mathbf{f} - \mathbf{g}\|^2_{\mathcal{D}_3}$. In effect it would be minimizing the area of $\mathcal{D}_3$ by trying to fit the reflected image to the original image with as little nonoverlapping area as possible. Such a solution is shown in Fig. 4(b) where the detected MSP is placed to the left of the actual (defined) MSP. It is still true that a large contribution to $\|\mathbf{f} - \mathbf{g}\|^2$ comes from $\mathcal{D}_3$, but now the nonoverlapping region is smaller so that $\|\mathbf{f} - \mathbf{g}\|^2$ is also smaller. Clearly, the way to avoid this problem is to ignore the contribution from $\mathcal{D}_3$. This is achieved by defining the similarity measure in terms of $\mathbf{f}'$ and $\mathbf{g}'$, as prescribed in Section II-A, so that only points within $\mathcal{D}_1$ are considered.

A pertinent question is how this algorithm performs in the presence of asymmetries in the image which are due to clinical conditions. The modified symmetry measure used in this paper is designed to handle cases where the image intensity in the asymmetric regions falls below the threshold level T (e.g., missing data). However, if the intensity is above the threshold, it will be included in $\mathbf{f}'$ and $\mathbf{g}'$ and thus decrease $s(\mathbf{f}', \mathbf{g}')$. Nevertheless, in our experience such regions are only a small fraction of the image volume and the remaining symmetric regions will be sufficient to guide the algorithm into finding an accurate set of parameters. In the case of gross asymmetry, the underlying assumption of our algorithm that the MSP divides the brain into two *almost* symmetric halves is violated. One example

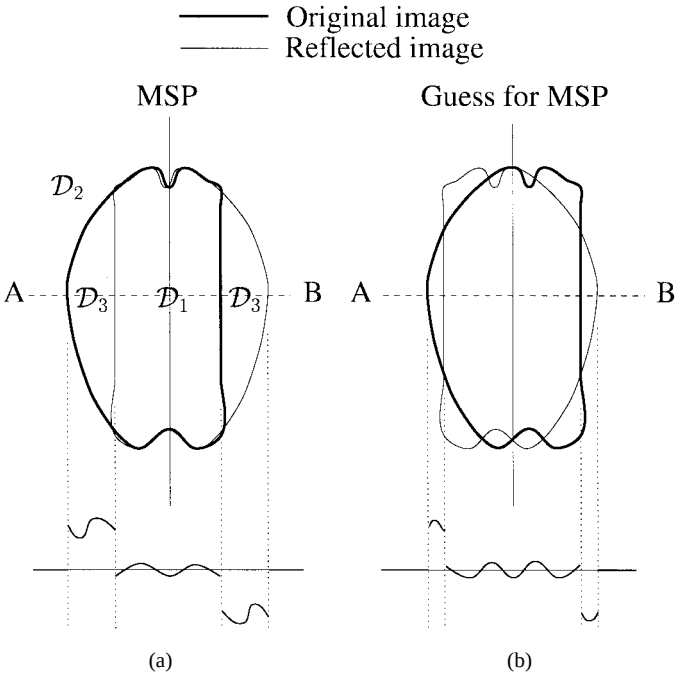

Fig. 4. An illustration of how missing data can cause the similarity measure $s(\mathbf{f}, \mathbf{g})$ to yield an inaccurate MSP. In (a) the MSP is placed at its best possible position and in (b) it has been moved to the left. Also in (a), $\mathcal{D}_1$ marks the region where *both* the original image and its reflection are above the threshold T, $\mathcal{D}_2$ is the region where *neither* is above the threshold, and $\mathcal{D}_3$ where *only one* is above the threshold. Similar regions can be assigned for (b).

where the algorithm failed is presented in Fig. 2. This provides an idea of the extent of asymmetry that must exist for failure to occur.

As pointed out in Section II-C, the choice of the initial plane for optimization is crucial to the success of the algorithm. Therefore, any method that improves the initial guess for the location of the MSP will enhance the performance of the program. In this paper, the method of selecting the starting point for the optimization algorithm relies on two steps. First, the choice of the initial plane is limited to those that pass through the computed center of mass of the image. Second, from a large number of random selections amongst these planes, we choose the one that produces maximum cross correlation as computed on an image of reduced size. Although we have not explored this further, one suggestion for improving the initial guess is to use the principal axes of the image [10].

V. Conclusions

In this paper, we have described a technique which locates the MSP of a 3-D brain image. The algorithm is independent of the imaging modality and is truly 3-D in the sense that it is insensitive to the initial orientation of the image in space. The technique finds the plane which divides the image into two regions (one on either side) with maximum symmetry. The measure of symmetry is a cross-correlation function. The key to the success of the algorithm is twofold. First, careful attention is paid to the construction of the vectors used in the symmetry measure so that certain undesirable solutions are avoided. Second, the search of the parameter space is performed on smaller images with lower resolution. The use of smaller images dramatically reduces the computational cost while still producing satisfactory results.

When applied to a large number of clinical images, the results were satisfactory in 19 out of 20 patients. The one patient for which the program failed had gross asymmetries in the brain and skull. The algorithm also performs satisfactorily for MR and PET images scanned from animals.

References

[1] J. L. Lancaster, T. G. Glass, B. R. Lankipalli, H. Downs, H. Mayberg, and P. T. Fox, "A modality-independent approach to spatial normalization of tomographic images of the human brain," *Human Brain Mapping.*, vol. 3, pp. 209–223, 1995.

[2] S. Minoshima, R. A. Koeppe, K. A. Frey, and D. E. Kuhl, "Anatomic standardization: Linear scaling and nonlinear warping of functional brain images," *J. Nucl. Med.*, vol. 35, no. 9, pp. 1528–1537, Sept. 1994.

[3] I. Kapouleas, A. Alavi, W. M. Alves, and R. E. Gur, "Registration of three-dimensional MR and PET images of the human brain without markers," *Radiol.*, vol. 181, pp. 731–739, 1991.

[4] E. Shimosegawa, J. Hatazawa, A. Inugami, H. Fujita, T. Ogawa, Y. Aizawa, I. Kanno, T. Okudera, and K. Uemura, "Cerebral infarction within six hours of onset: Prediction of completed infarction with Technetium-99m-HMPAO SPECT," *J. Nucl. Med.*, vol. 35, no. 7, pp. 1097–1103, July 1994.

[5] L. Junck, J. G. Moen, G. D. Hutchins, M. B. Brown, and D. E. Kuhl, "Correlation methods for the centering, rotation, and alignment of functional brain images," *J. Nucl. Med.*, vol. 31, no. 7, pp. 1220–1226, July 1990.

[6] S. Minoshima, K. L. Berger, K. S. Lee, and M. A. Mintun, "An automated method for rotational correction and centering of three-dimensional functional brain images," *J. Nucl. Med.*, vol. 33, no. 8, pp. 1579–1585, Aug. 1992.

[7] M. E. Brummer, "Hough transform detection of the longitudinal fissure in tomographic head images," *IEEE Trans. Med. Imag.*, vol. 10, pp. 74–81, Mar. 1991.

[8] A. Venot, J. C. Liehn, J. F. Lebruchec, and J. C. Roucayrol, "Automated comparison of scintigraphic images," *J. Nucl. Med.*, vol. 27, no. 8, pp. 1337–1342, Aug. 1986.

[9] W. H. Press, S. A. Teukolsky, W. T. Vetterling, and B. P. Flannery, *Numerical Recipes in C.* New York: Cambridge Univ. Press, 1992, pp. 408–412.

[10] N. M. Alpert, J. F. Bradshaw, D. Kennedy, and J. A. Correia, "The principal axes transformation—A method for image registration," *J. Nucl. Med.*, vol. 31, no. 10, pp. 1717–1722, Oct. 1990.